

Machine Learning to Enable Orders of Magnitude Speedup in Multi-Objective Optimization of Particle Accelerator Systems

Auralee Edelen¹, Andreas Adelman², Nicole Neveu¹, Yannick Huber², Matthias Frey²

¹*SLAC National Laboratory, Menlo Park, CA, USA*

²*Paul Scherrer Institut, Villigen, Switzerland*

High-fidelity physics simulations are powerful tools in the design and optimization of charged particle accelerators. However, the computational burden of these simulations often limits their use in practice for design optimization and experiment planning. It also precludes their use as online models tied directly to accelerator operation. We demonstrate an approach based on machine learning to create nonlinear, fast-executing surrogate models that are informed by a sparse sampling of the physics simulation. The models are accurate and are $\mathcal{O}(10^6)$ more efficient to execute (e.g. < 1 ms on a laptop). Beyond this, we demonstrate that these models can be reliably used with multi-objective optimization to obtain substantial speedup in initial design studies (e.g. requiring 262x fewer simulation evaluations to obtain an equivalent solution). This approach enables new ways for high-fidelity particle accelerator simulations to be used, both for experimental operation and for more thorough design studies, at comparatively low computational cost.

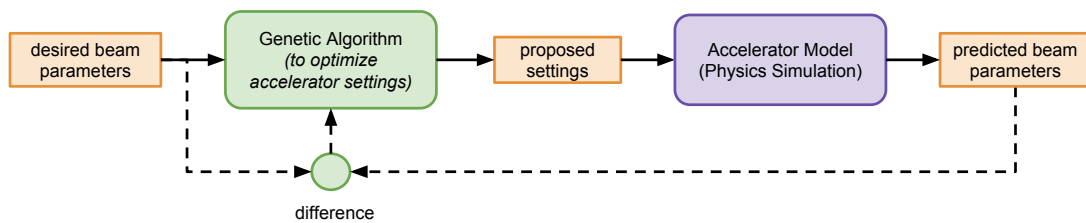
Motivation

High-fidelity physics simulations are essential tools for both the initial design and subsequent optimization of modern particle accelerator systems. Because they require complex beam behavior to be taken into account (e.g. instabilities, nonlinear collective effects, beam self-fields), standard codes used for this task (e.g. OPAL ¹, IMPACT ^{2,3}, ASTRA ⁴, WARP ⁵) are often computationally intensive to run. Exacerbating this computational burden, accelerator systems often consist of many components that can be used to accelerate and manipulate the beam (e.g. accelerating cavities, bending and focusing magnets). Along with these come many controllable variables that can be independently adjusted to achieve specific particle beam characteristics. In many cases, the subtle nonlinear interactions between all of these variables must be considered when trying to predict the behavior of the beam. This makes modeling these systems from “start-to-end” (i.e. from the beginning of the accelerator where the particle beam is created to a point of interest) critical for obtaining realistic predictions. As a result, detailed design and optimization studies for particle accelerator systems often require the use of thousands of cores at High Performance Computing (HPC) facilities. While in principle many large accelerator facilities have access to such resources, in practice this computational burden significantly hampers efforts to conduct thorough optimization studies where many individual evaluations of the simulation must be made.

Optimization of this nature is important in the initial design of particle accelerator systems when many tradeoffs between possible setting combinations must be explored. In practice, multi-objective optimization using genetic algorithms is frequently used for finding optimal setting com-

binations (e.g. see Figure 1). Accelerator physicists use the resultant Pareto fronts^{6,7} to examine trade-offs between achievable beam parameters and inform design choices (see for example⁸⁻¹⁰). For existing designs, thorough offline optimization of settings using high-fidelity simulations can also aid in experiment setup and planning. This is especially the case for facilities that require frequent re-tuning of settings or exploration of novel experimental setups. For example, at free electron laser (FEL) facilities like the Linac Coherent Light Source (LCLS) and Swiss Free Electron Laser (SwissFEL), user requests for specific beam parameters must be handled quickly and efficiently, and novel FEL schemes are often developed during limited blocks of time in between user operations.

Figure 1: Genetic algorithms are frequently used in the optimization of particle accelerator settings to achieve the required particle beam parameters. The use of multi-objective optimization, in which multiple output variables are considered simultaneously, enables optimal trade-offs between different beam parameters to be examined explicitly.



At present, even though high-fidelity physics simulations are often created as part of the initial design process for a new accelerator, they are often not fully utilized during machine operation (i.e. as “online models”) for use in live machine optimization and control. This is largely because their execution speed is too low. Instead, online models tend to rely on greatly simplified representations of the physics (e.g. see¹¹⁻¹³), and as a result trade accuracy for speed. In a few exceptional

cases, higher-fidelity models are used to aid operation, particularly when on-site HPC resources are available ¹⁴⁻¹⁶. However, the use of high-fidelity simulations with a fine mesh and large number of particles directly to aid operation remains a rarity.

In light of these limitations, improving the execution speed and scalability of particle accelerator simulations is an area that has seen considerable effort in recent years ^{17,18}. Approaches to do this have focused on parallelization and hardware-based acceleration (e.g. using GPUs) of existing simulation codes ^{19,20}. This includes OPAL ²¹, the accelerator physics simulation code used in this study. Improvements to underlying modeling algorithms, such as using the Lorentz boosted frame ²² and spectral solvers ^{23,24}, have also provided orders of magnitude increases in computation speed. All of these efforts are highly successful. However, it remains the case that the computational expense of these codes still limits them from being fully utilized by the accelerator community.

Here we investigate a different, but complementary, approach that immediately enables new capabilities in how these existing high-fidelity physics simulations can be used by the particle accelerator community. We show that one can create Machine Learning (ML) based surrogate models to obtain an accurate, fast-executing representation of the relevant beam dynamics from a sparse sampling of accelerator physics simulations of interest. In contrast to the physics simulations, these surrogate models can execute in fractions of a second on a laptop with comparable accuracy in predicting the resultant beam parameters. We further show that these models are useful for multi-objective optimization in two important ways: (1) they accurately reproduce optimiza-

tion results obtained from the physics simulation, meaning they can be reliably used in experiment planning and live optimization during accelerator operation and (2) they can be used to substantially speed up the initial design optimization process without the need to run an optimization algorithm entirely on the computationally intensive physics simulation.

We demonstrate the approach using OPAL simulations of a linear accelerator at the Argonne Wakefield Accelerator (AWA) Facility ²⁵. Research at the AWA is focused on advanced accelerator concepts, which generally include efforts to improve accelerator operations, diagnostics, and components (such as accelerating structures) for future accelerators. Much effort is also spent on developing and testing beamline configurations that could be used for beam shaping ²⁶, or future linear colliders ²⁷. Often, the accelerator settings (e.g. focusing fields for all magnets, cavity phases, cavity accelerating gradients) are adjusted prior to each experiment to achieve custom beam characteristics (e.g. beam energy spread, transverse sizes). The accelerator also operates at bunch charges where nonlinear effects are important (e.g. 40 nC), and the cavity fields contain asymmetries. Overall, this results in a challenging optimization problem, and 3D particle-in-cell (PIC) simulations are required to accurately predict the beam behavior.

Multi-objective optimization using genetic algorithms (GAs) is common in the accelerator community, therefore we chose it as the standard for assessing the performance of our ML models. We compared the Pareto fronts obtained from running a GA with the *ML-based surrogate models* and those obtained by running a GA with the *physics simulation* (OPAL) and find that these are in good agreement. In addition, we show that running a GA with the ML model in some cases

actually provides a more accurate estimate of the true Pareto front than naively running a GA with the physics simulation. We further demonstrate that only a sparse sampling of the parameter space from the physics simulation is needed in order to create an accurate ML model (a few hundred samples in our case). Based on these results, we suggest a new procedure for doing multi-objective optimization in particle accelerators that provides many orders of magnitude increase in computation speed while retaining a high degree of accuracy.

This approach enables high-fidelity representations of the physics simulation to be encapsulated in a fast-executing form, thus enabling their use as online models. Such models are more accurate than the simplified physics models that are presently used when fast execution is needed. ML models have been used by the authors in several previous instances to create fast-executing surrogates for computationally intensive accelerator simulations^{28–30}. The main difference to previous work is the rigorous evaluation of such models for use in multi-objective optimization using genetic algorithms, the comparison between different ML models, and an evaluation of how many training samples are needed to obtain an accurate model when used with optimization algorithms. In addition, although we do not address it in this case, these models can in principle be updated with machine measurements (e.g. see³¹) to help improve model fidelity with respect to the real machine behavior. These results should encourage the accelerator community to adopt ML-based surrogate modeling as a standard way of creating fast-executing, accurate accelerator models from high-fidelity physics simulations, especially for design optimization and online modeling. For brevity in subsequent text, we use the term “physics simulations” for the high-fidelity OPAL simulations of the AWA, and we refer to the multi-objective genetic algorithm used in this study (NSGA-II³²),

as the “GA.”

Results

Description of ML Surrogate Modeling Approach The approach consists of training a ML model on a sparse random sample from the computationally expensive physics simulation (see Figure 2 for more detail). The training data consists of random combinations of controllable input variables on the accelerator and the resultant beam parameters predicted from the physics simulations.

To assess the performance of the ML model when used with an optimization algorithm, we run a GA with the physics simulation to optimize settings (e.g. rf cavity phases, rf cavity gradients, solenoid strengths). We then run a GA with the ML model and compare the resultant Pareto fronts (for the workflow see Figure 3). Good agreement between the Pareto fronts indicates that the ML model can be used as an accurate replacement for the physics simulation in multi-objective optimization, despite only using a sparse sampling of the parameter space to learn a representation of the underlying physical behavior.

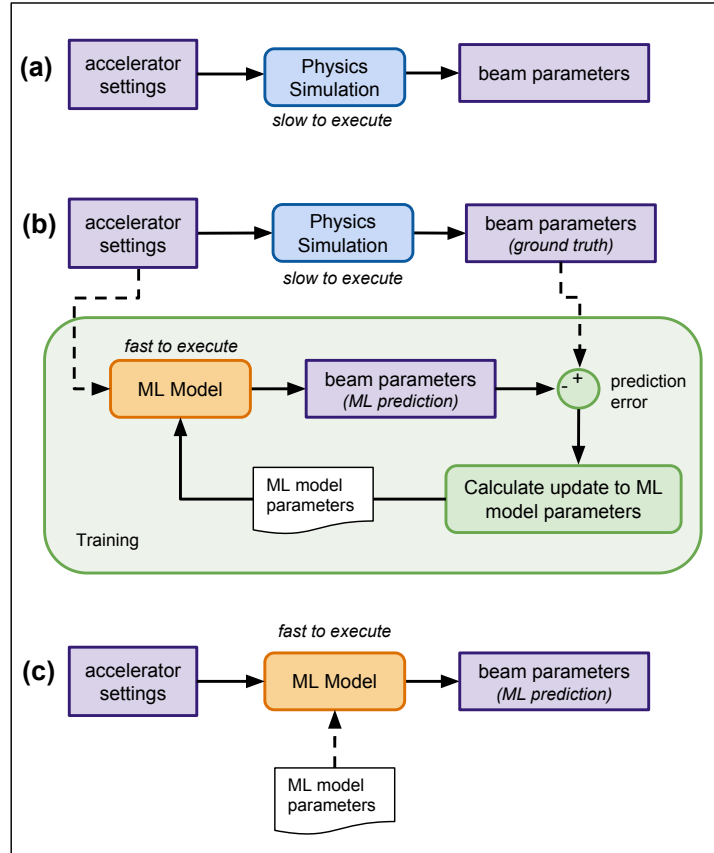


Figure 2: Approach to train ML-based surrogate models with computationally expensive, high-fidelity particle accelerator simulations. Initially, we have a slowly-executing physics simulation that we can use for beam parameter prediction and design optimization (a). We then use the physics simulation to generate a training data set for the ML model (e.g. selecting a sparse random combination of accelerator settings and simulating these cases). The ML model parameters are then optimized until the ML model predictions of the beam parameter match those from the physics simulation sufficiently closely (b). At the end of the process we obtain a fast-executing representation of the physics simulation that can be used for optimization and online modeling (c).

Approach for Validating ML Model Performance Under Optimization

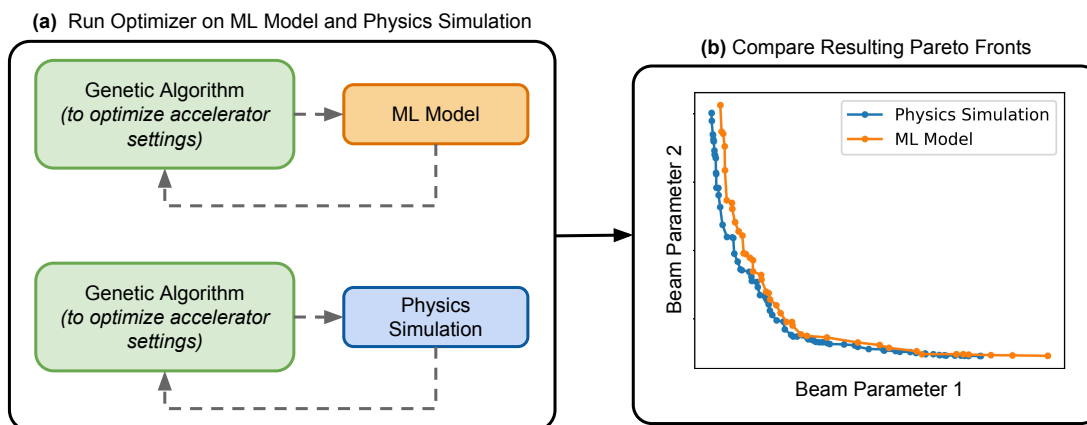


Figure 3: Approach for assessing reliability of ML-based model performance when used in optimization of accelerator settings. We run a GA with the physics simulation to find accelerator settings that optimize the beam parameters. We repeat this optimization with the ML model instead of the physics simulation. In a last step, the Pareto fronts from the GA are compared. A close match in the Pareto fronts indicates that a high degree of accuracy is achieved and the ML model is a reliable surrogate for the physics simulation when used in conjunction with an optimization algorithm.

Validation of ML Surrogate Modeling Approach We demonstrate the efficacy of our approach by training ML models on a sparse random sample of six adjustable input variables (i.e. accelerator settings) for the AWA and seven of the resultant beam parameters (see Figure 4). The inputs were varied uniformly over a subset of the operating range of the accelerator (see Table 3). For the GA based optimization of the beam parameters, the same range of input variables was allowed, but actual distribution is determined by the way in which the GA traverses the parameter space. We repeated this process for two different bunch charges, 1 nC and 40 nC. Details on the data sets, training procedures, specific implementations of the ML models, the implementation of the GA, and the physics simulations can be found in the “Methods” section. In terms of ML model choice, we focus on Artificial Neural Networks (ANNs) to demonstrate the techniques, but also conduct a comparison with Polynomial Chaos Expansion (PCE) surrogates.

We find that the Pareto fronts obtained using the ML models and the physics simulation are in good agreement. As representative examples, in Figure 5 we show the comparison for the ANN model and the physics simulation for several key beam parameters. In this case, only 5k random sample points were used in training. However, the GA run on the ANN is still able to generate a set of Pareto fronts that is very close to those obtained with the physics simulation (the latter of which required 131k simulation evaluations). Furthermore, only a small amount of fine-tuning of the ANN architecture was done in this case, as the initial topology and hyperparameters were chosen based on previous experience of the authors with similar types of injector modeling problems^{28,29,31}. This highlights the generality of this approach for common problems in accelerator physics and hints at the possibility for doing transfer learning with the produced models.

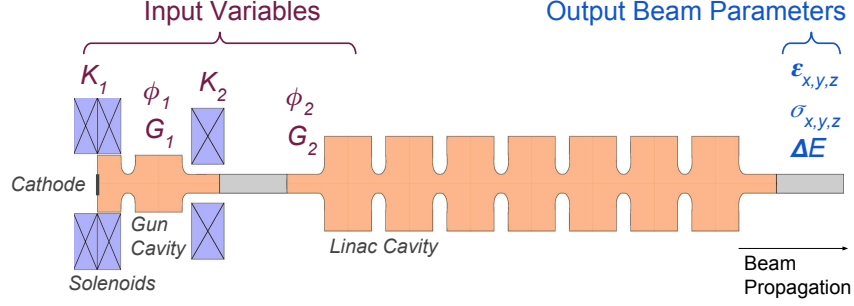


Figure 4: Schematic of the AWA linac, along with the controllable accelerator settings and predicted beam parameters. The randomly-varied inputs include the injector rf phase ϕ_1 and accelerating gradient G_1 , the linac cavity rf phase ϕ_2 and accelerating gradient G_2 , and two solenoid strengths K_1 and K_2 . The output electron beam parameters are the transverse spot sizes σ_x and σ_y , the bunch length σ_z , the transverse projected emittance values ε_x and ε_y , the longitudinal projected emittance ε_z , and the energy spread ΔE . The input variable ranges are determined by typical operating ranges at the AWA and are shown in Table 3. We examined this setup for two bunch charges: 1 nC and 40 nC. Each bunch charge has an appropriate value for the radius of emission on the cathode that was previously determined (these are 2 mm and 9 mm, respectively).

Extension to Initial Design Optimization Assuming the physical function to be modeled is smooth and that the ANN is learning a good representation of the underlying physical system, running the GA with the ANN may actually provide a more accurate estimate of the true Pareto front than naively running a GA with the physics simulation. For example, this could happen if the GA cannot in practice run for a sufficient number of generations or with a large enough population to converge. This can easily be the case when HPC resources are limited and/or the optimization problem is high-dimensional. In contrast, the computationally cheap execution of the ANN en-

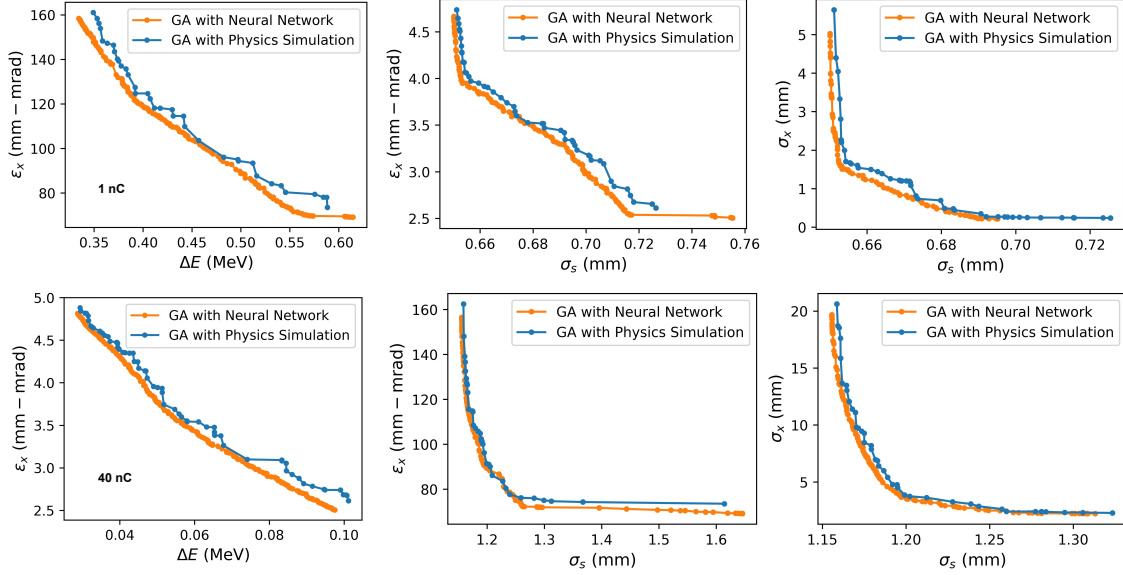


Figure 5: Representative examples of comparison between Pareto fronts for 1 nC (top row) and 40 nC (bottom row) obtained by running a GA with the physics simulation and with the ANN based surrogate model.

ables more individuals to be used in the population and a greater number of generations to be run. To explore this further, we ran the inputs corresponding to the predicted Pareto points (i.e. those generated via running a GA with the ANN) through the physics simulation. Upon inspection, the points on the Pareto front from the ANN match the results from the physics simulation very well (see Figure 6). This indicates that the ANN has indeed learned an accurate representation of the underlying physical system, and that the estimate of the Pareto front obtained is *closer to the true Pareto front* than that obtained from naively running a GA with the physics simulation. This is different than merely interpolating between points seen in the training data set, as the ANN was able to predict more optimal combinations of parameters in a region of parameter space that was not explicitly represented in the training data.

Examining this particular case more closely, we see that with 200 generations, the GA run with the physics simulation may not have fully converged (observe in Figure 6 that the front is not very smooth). To get a rough approximation of how much additional convergence could be expected, we ran another GA with the physics simulation, this time with 500 generations (see Figure 7). We see that it converges more closely to the best observed Pareto front; however, the Pareto front found with the ANN is still the best-known optimal solution.

Taken together, these results highlight another advantage of our approach: in addition to creating a fast-executing representation of the physics simulation, the ML model can be used to speed up initial optimization (i.e. for finding new optimal solutions from a simulation that has not yet been fully explored). This can be done in a few key steps that start with training the ML model on a sparse random sampling of the simulation, and running a GA with the ML model. The resulting inputs corresponding to the Pareto front obtained with the ML model can then be used as an initial population for a subsequent GA run with the physics simulation to fine-tune the result (see Figure 12). In addition to being more computationally efficient, a larger generation and population size could be used with the ML model than would normally be feasible with the physics simulation, thus potentially enabling more optimal solutions to be found.

While training an ML model as an intermediate step in the optimization process may seem cumbersome, GAs do have their own hyperparameters that need to be tuned (e.g. population size, number of generations, crossover and mutation probabilities). The risk of wasting computational resources while tuning these parameters is high. Some of these could instead be initially tuned

with the ML model. In addition, the computational cost of the parameter space exploration with the GA before it gets close to convergence is high. Using the ML model enables one to skip these early stages of convergence.

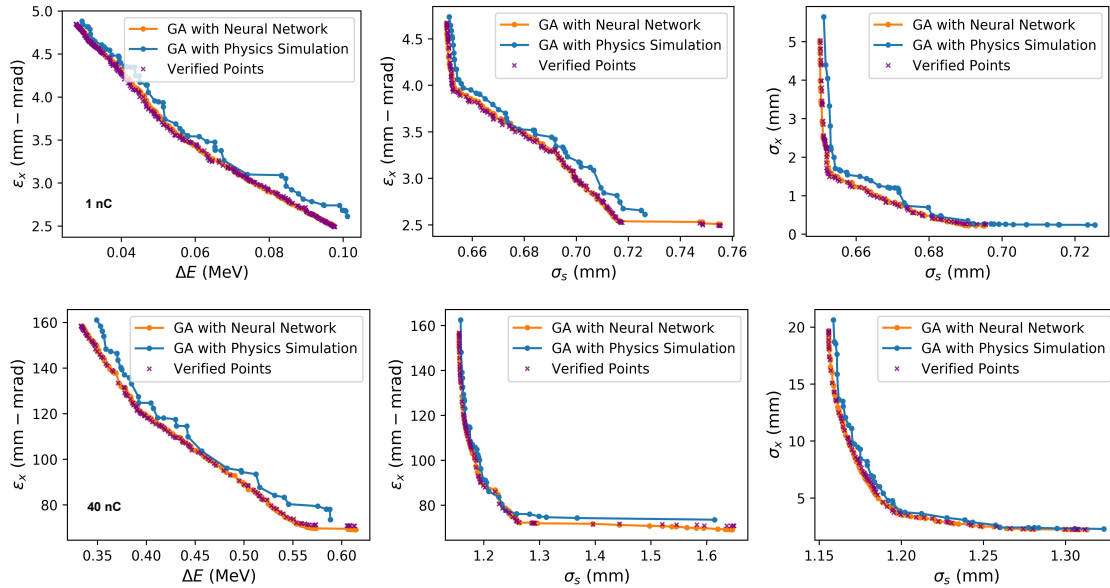


Figure 6: For both bunch charges examined, 1 nC and 40 nC, the original Pareto front from running the GA with the physics simulation and with the ANN are shown, along with the result of using the physics simulation to verify points from the Pareto front suggested by the ANN. The results indicate that the ANN actually provided a better estimate of the true Pareto front than the GA run for 200 generations with the physics simulation.

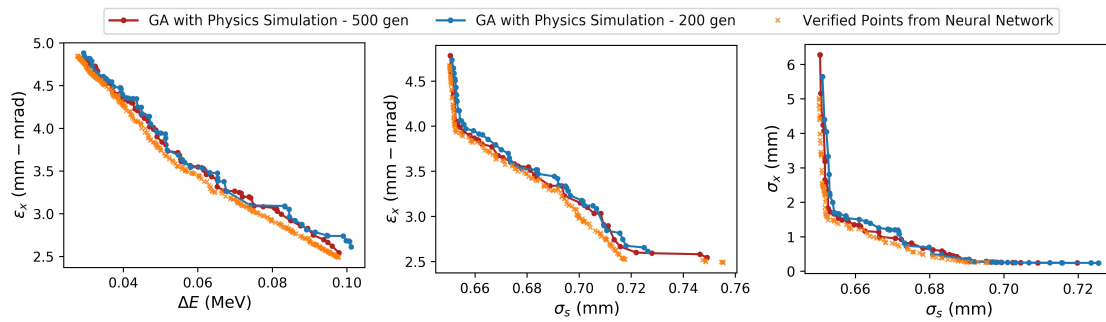


Figure 7: Comparison between Pareto fronts for 1 nC obtained by running GA with the physics simulation for 200 generations, running GA with the physics simulation for 500 generations, and running GA with the ANN for 200 generations. For the ANN we show the points that we verified with the physics simulation.

Impact of Training Sample Size Generating training data using the physics simulation is expensive. In light of this, one question which naturally arises is how the accuracy of the ML model will change with the number of samples used in training. This is important for estimating the corresponding trade-off between computation time needed to generate the training set (a limited resource) and the resultant model accuracy (the requirements for which may vary depending on the application).

To address this, we trained models using 5k, 500, 200, and 100 points from the random sample set and then compared the resulting Pareto fronts obtained using each of these (see Figure 8). Note that even when using only 500 points we do not see substantial reduction in the Pareto front accuracy. For training with 200 points, it starts to deviate more substantially, but the solution is still close enough to be used as a warm start for subsequent fine-tuning with the physics simulation.

In order to visualize the extent to which the ML model is generalizing to new regions of the parameter space (as opposed to just learning the Pareto front directly from the training data), we examined the sampled points directly. This gives us a rough approximation of the hypervolume projections, which correspond to the projected area of the parameter space explored by the GA and by the random sample (see Figure 9). From this we see that the random sample covers a smaller area of the parameter space than that covered by the GA (meaning the training data does not cover the entire space). We also see that the GA run with the ML model smoothly fills out the parameter space explored in the physics simulations, and indeed, extrapolates beyond it.

As an additional visualization, we trained ML models on a larger range of training sample

sizes and evaluated their performance in predicting the physics simulation results (see Figure 10). All training samples are drawn from the same overall random sample distribution (consisting of 70k points in total), and the prediction performance is evaluated on the GA samples from the physics simulation. We quickly see diminishing returns in improvement for the prediction task after increasing the number of samples beyond a few thousand.

How this scales to accelerator systems with a greater number of input/output variables, wider variables ranges, or more complex dynamics will need to be addressed in future work. However, injector systems that are similar in scale and complexity to the AWA are extremely common, and these results should provide good guidance for those wishing to use this method on similar systems. As many beam dynamics problems in accelerators are similar, it is also reasonable to expect that these results could provide good starting points for applying these techniques on other kinds of accelerator systems.

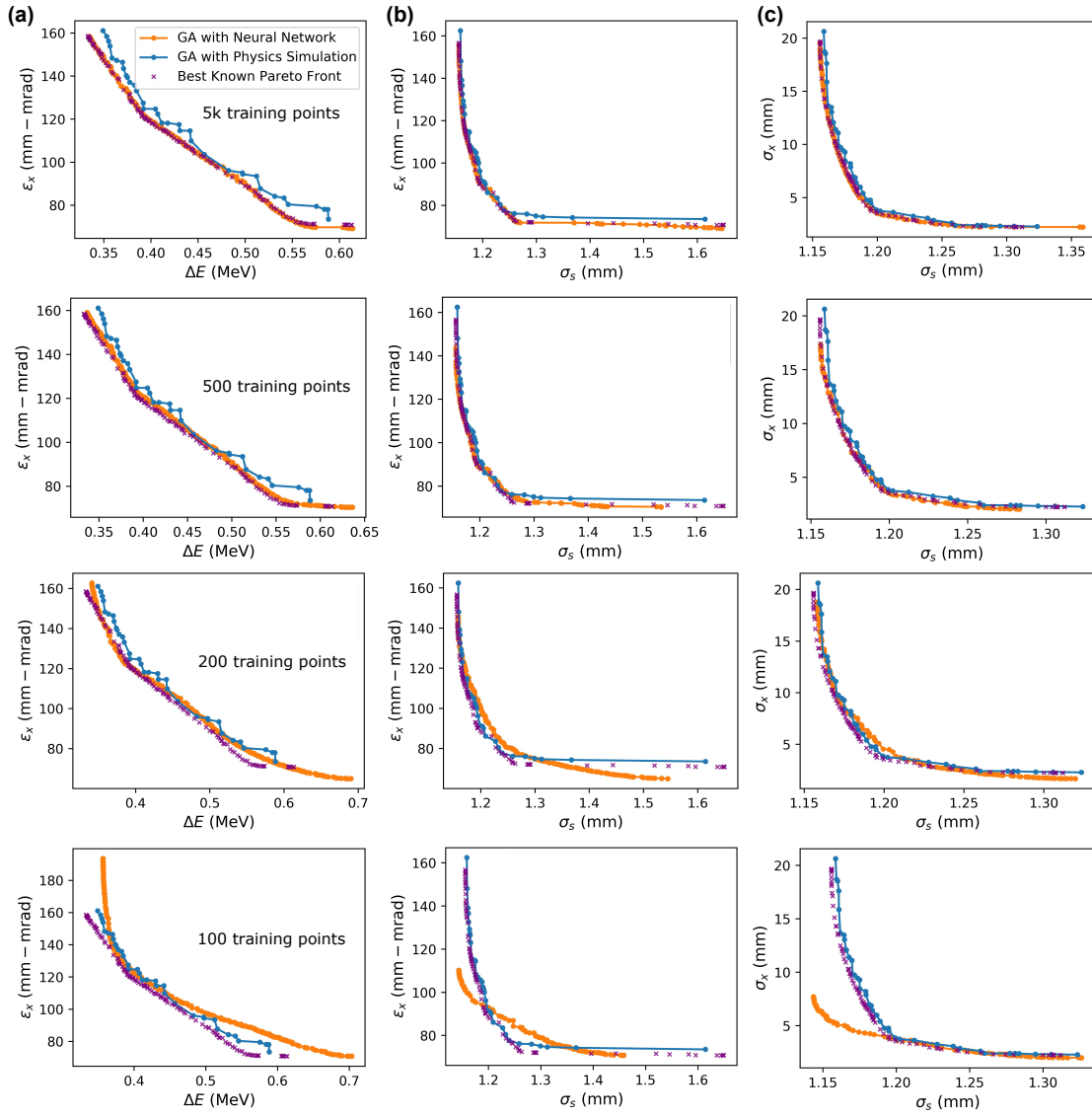


Figure 8: Impact of training set size on the Pareto front obtained from the neural network for three sets of Pareto fronts in the 40nC case: ΔE vs. ε_x (a), σ_s vs ε_x (b), and σ_s vs σ_x (c). Cases with 5k, 500, 200, and 100 training points are shown from top to bottom.

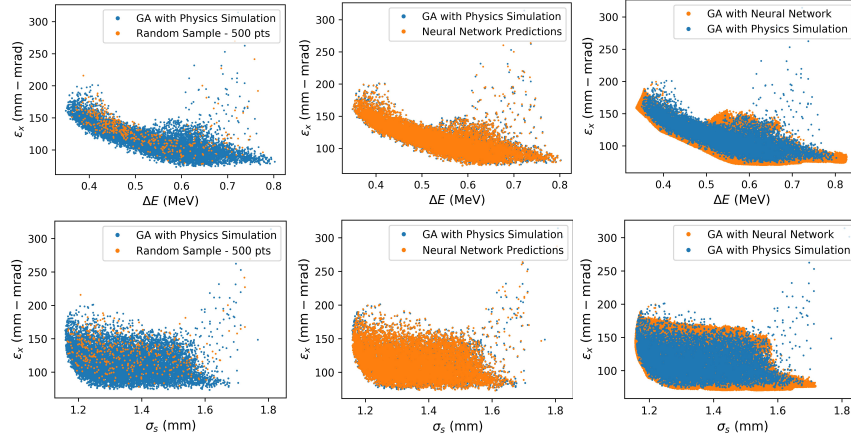


Figure 9: Representative examples of sampled points (approximate hypervolume projections). The overlap between the random sample training data and the data from running the GA with the physics simulation is shown at left. Here we also show the final Pareto front from the ANN, as verified with the physics simulation. After training on the random sample, the ANN is able to predict with high accuracy the points sampled from running the GA with the physics simulation (middle column). Finally, we show the result of running the GA with the ANN. We see that it smoothly fills out the space observed from running the GA with the physics simulation and indeed generalizes beyond it (right column).

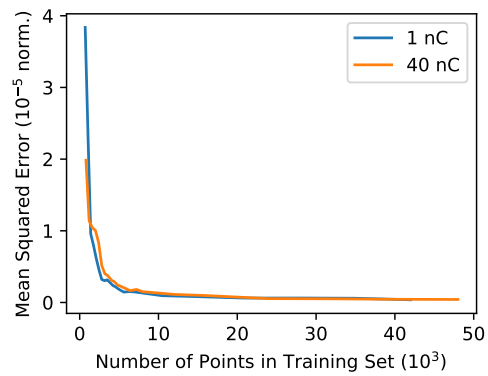


Figure 10: Impact of random sample training set size on model prediction accuracy for the GA test set. In this case, the error in predicting the GA samples is used, rather than the error in the Pareto front obtained from optimization with the ML model. The values shown are in terms of normalized units (i.e. data has been scaled to fit within the range -1 to 1).

Improvement in Computational Efficiency Gained by Using ML Model In Table 1, the time-to-solution and computing resources needed for GA optimization using the physics simulation are compared with those needed for GA optimization with the ANN-based surrogate model. The ANN-based GA optimization is $\mathcal{O}(10^3)$ faster in terms of time-to-solution than the physics simulation based optimization and takes about 2 minutes on a *laptop computer* (in this case, one core of an Intel Core i7 processor). This corresponds to $\mathcal{O}(10^6)$ times fewer computing resources (in terms of core hours).

	Time to solution (hours)		Resources (core-hours)	
	1 nC	40 nC	1 nC	40 nC
GA with physics simulation using 2246 cores	16.57	36.04	43778	95218
GA with ANN model using 1 core	0.033	0.033	0.033	0.033
Factor improvement using ANN model	$0.5 \cdot 10^3$	$1.09 \cdot 10^3$	$1.33 \cdot 10^6$	$2.89 \cdot 10^6$

Table 1: Comparison of time-to-solution and computing resources for running the GA with physics simulation and the GA with the ANN.

Once training is completed, the ANN model evaluation can be completed in under a millisecond on a laptop computer, compared with 255 seconds for one physics simulation on 8 cores. This is a speedup of $\mathcal{O}(2.55 \times 10^5)$ and opens the door for high-fidelity, fast-to-execute accelerator models. Importantly, the overall speedup is still substantial when considering the computation time required to generate the training data and to train the ANN.

Running the GA with the physics model using 2246 cores in the 1 nC case took approximately 42,510 core hours on 2,624 cores at the Laboratory Computing Resource Center (LCRC)³³ at ANL, with a time-to-solution of 16.6 hours and 131,010 simulation evaluations. To generate a random sample for training, only 500 evaluations of the physics simulation are needed to still maintain a high degree of accuracy (i.e. 262x fewer simulation evaluations). In terms of computation time, with 2,624 cores this takes approximately 6.4 minutes using the above mentioned computing system and physics simulation setup. Finally, the ANN training takes approximately 10 minutes on one core of an Intel Core i7 processor. Furthermore, for a given problem, this step of generating the data and training the model only needs to be done once, and the ANN model can be used for subsequent modeling and optimization tasks.

It is important to note that in our case we conducted a massively parallel physics simulation with the beam dynamics code OPAL, which has been optimized for HPC systems. Even so, we still see substantial improvement in computational efficiency using the ML model. In cases where codes are less efficient or higher complexity, this approach may actually enable larger optimization studies to be conducted than would have been feasible using the physics simulation alone.

Comparison of Different Surrogate Modeling Methods We focused on comparing the performance of two kinds of ML models: feed-forward ANNs^{34,35} and polynomial chaos expansion models (PCEs)^{30,36}. As a quick check to see whether a linear model would be sufficient, we also trained a support vector regression (SVR) model³⁷ with a linear kernel. The mean square error over all predicted beam parameters using the SVR model was $5.5 \cdot 10^{-06}$, in comparison to $3.5 \cdot 10^{-10}$

for the ANN model, indicating that we do gain accuracy with a nonlinear model.

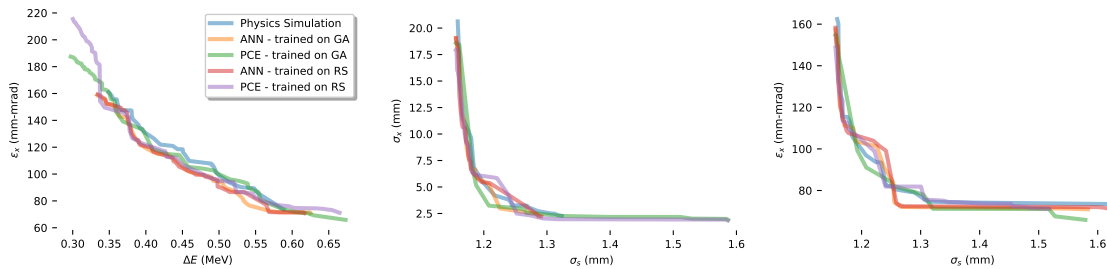
The ANN models produce more accurate predictions than the PCE models; however, one downside of using a simple ANN model is that it does not inherently give an estimate of prediction uncertainty and model sensitivity without additional analysis. In contrast, the PCE model has the benefit of immediately providing straightforward estimates of prediction uncertainty and sensitivity via the Sobol’ indices ^{30,38}. This is particularly advantageous when considering how these models may be used in design and online optimization of the running accelerator (for example, one might want an uncertainty estimate on an output parameter when deciding to set the machine to the corresponding input parameters). The PCE model also has fewer hyperparameters to tune (i.e. polynomial order, type of polynomial used). The execution of the ANN and PCE models are on the same order; hence *all* previous arguments made with regard to improved execution efficiency also apply to the PCE models.

Metric	PCE	ANN
1 nC Average Mean Squared Error	$1.6 \cdot 10^{-07}$	$3.5 \cdot 10^{-10}$
40 nC Average Mean Squared Error	$4.5 \cdot 10^{-06}$	$2.9 \cdot 10^{-08}$
1 nC Average Standard Deviation	$3.3 \cdot 10^{-07}$	$5.5 \cdot 10^{-10}$
40 nC Average Standard Deviation	$8.4 \cdot 10^{-06}$	$2.3 \cdot 10^{-08}$

Table 2: Comparison of mean squared error and standard deviation of all predicted beam parameters obtained with different models. This shows predictions for the GA samples. The 70k random sample was used to provide the training set.

We also compared the results obtained when training on a subset of the GA sample data (as opposed to training on random sample data). In some cases accelerator scientists may already have samples available from prior GA runs on a physics simulation and could use that data set directly to train a surrogate model. Since the GA has already been run, this is useful if the goal is mainly to obtain a fast-executing representation of the physics simulation (rather than speed up the initial design optimization). In Figure 11, we show a comparison between the Pareto fronts obtained with the PCE and the ANN.

Figure 11: Pareto front comparisons for 1 nC and 40 nC. “ANN - trained on GA” and “PCE - trained on GA” refer to ANN surrogate models trained directly on a subset of the GA data. Similarly “ANN - trained on RS” and “PCE - trained on RS” refer to surrogate models trained on the random sample data. In this case, the entire random sample data is used (70k points) to provide the training, validation, and testing data.



Discussion

In practice, high-fidelity physics simulations for particle accelerators are often too slow for full exploration of the parameter space during optimization. The slow execution speed also prohibits their use concurrent to machine operation (i.e. as online models to aid accelerator operations). We have demonstrated that machine learning can be used to obtain a fast-executing representations

of particle accelerator physics simulations and that relatively little data is needed to achieve a high degree of fidelity relative to the original physics simulation (e.g., a few hundred samples in our case). The approach presented here provides one avenue toward creating fast-executing representations of physics simulations that can be used in machine operation, which would not otherwise be possible. In addition, we have shown that these models can be reliably used in GA based optimization. Beyond this, we showed that some classes of surrogate models are capable of providing a more accurate estimate of the true Pareto front when used in conjunction with a GA than naively running a GA with the physics simulation, and that this approach requires substantially fewer simulation evaluations than running a GA directly with the physics simulation (e.g. 262x fewer simulations in our case). This work thus opens up the possibility to do more extensive optimization than may otherwise have been feasible, both for new designs and for experiment planning with existing designs.

These results also suggest three particularly useful avenues for using this approach in particle accelerator applications. First, one can update the model learned in simulation with measurements from the machine to account for deviations between the simulation and the real machine behavior. This was shown to be viable in ³¹, but more rigorous study is needed. Second, one can begin to use these surrogate models directly in machine operation. In some cases, high-fidelity simulations can be made to match the machine very closely and can be used to provide suggestions for machine settings (for a comprehensive example, see ³⁹). If the simulation matches the machine closely enough, or the particular application does not need high accuracy, the ML model trained on the simulations can immediately be used to aid operations, without the need to update it with measured

data from the machine. Such models could aid machine operation by including them in online optimization procedures to help guide the search for optimal settings and in other model-based control routines. Machine operators could also check the potential impact of setting changes before trying them out on the actual machine. These models could also be used as a diagnostic tool to provide predictions about un-measured beam parameters or to flag when the system has changed substantially (i.e. if the model prediction suddenly does not match the machine). Finally, our results suggest a new procedure for doing GA optimization of particle accelerators. Instead of running a GA with the physics simulation, one can run a small random sample over the parameter space, train a surrogate model on this small sample, and run a full GA using the surrogate model very quickly. Then the Pareto points obtained from the surrogate model can be used as an initial population in a subsequent short GA with the physics simulation to verify and fine-tune the result (see Figure 12). Future work will also need to assess how well this approach scales accelerator systems with a greater number of input/output variables, wider variables ranges, and more complex system dynamics.

Methods

Data Sets for the Surrogate Models For each bunch charge (1 nC and 40 nC), we generated uniformly-distributed random simulation samples. For this we used the OPAL-based interface for creating such data sets, which was developed in part to support this effort. This feature allows the submission of massively parallel jobs using an OPAL input file. The randomly-varied inputs include the injector phase ϕ_1 and gradient G_1 , the linac cavity phase ϕ_2 and gradient G_2 , and two

solenoid strengths K_1 and K_2 . The output parameters are the transverse spot sizes σ_x and σ_y , the longitudinal beam size σ_s , the transverse projected emittances values ε_x and ε_y , the longitudinal projected emittance ε_s , and the energy spread ΔE . The input variable ranges are informed by the operating ranges at the AWA (see Table 3). Random samples for two bunch charges were generated (1 nC and 40 nC, with the corresponding laser radius being 2 mm and 9 mm). In the 1 nC case, we generated 70k samples, and in the 40 nC case, we generated 80k samples.

Name	Abbreviation	Min Value	Max Value	Unit
Solenoid 1 Strength	K_1	400	550	m^{-1}
Solenoid 2 Strength	K_2	180	280	m^{-1}
Injector Phase	ϕ_1	-10	0	deg
Cavity Phase	ϕ_2	-10	0	deg
Injector Accelerating Gradient	G_1	60	75	MVm^{-1}
Cavity Accelerating Gradient	G_2	15	25	MVm^{-1}

Table 3: Range of the AWA Input Variables.

The implementation of NSGA-II³² that is provided within OPAL was used for the GA with the physics simulation. Details related to the algorithm can be found in⁴⁰. We choose an initial population of 656 individuals and subsequently evolve the population over 200 generations, while retaining approximately the same number of individuals in each generation (occasionally fewer are retained by the algorithm). The following hyper-parameters were used: gene mutation probability $P_g = 0.8$, mutation probability $P_m = 0.8$ and recombination probability $P_r = 0.2$. Specific

descriptions of the hyperparameters can be found in Section 1.4.2 of the OPAL manual ¹, and the values used in this case were chosen based on previous optimization work for the AWA that involved a hyperparameter scan ¹⁰. The constraints of the MOO problem were set such that the variables stayed within the operating ranges of the AWA (see Table 3). For each generation, the input and output parameters from the simulation are saved. In the 1 nC and 40 nC cases respectively, 131,010 and 131,078 final samples were obtained.

OPAL Simulation OPAL ¹ is an open source library for conducting large-scale electrostatic Particle-in-Cell (ES-PIC) simulations of particle accelerators. For parallel execution, it uses MPI. For particle evolution in time, a fourth order Runge-Kutta or second-order Leapfrog algorithm with the Vlasov equation can be used. 3D space charge forces are calculated throughout the time-evolution of the beam. To calculate the self-field of the beam, a FFT Poisson solver is used in the beam rest frame. The particle generation at the CsTe photo-cathode is modeled using an uniform emission model, assuming a planar ideal surface. The laser profile used for emission is uniform transversely and a flattop longitudinally, with Gaussian tails. The full width half maximum of the laser in the longitudinal direction was 6 ps for both cases. The laser radius was set to 2 mm for 1 nC simulations. Due to large nonlinear space charge forces at 40 nC, the laser radius was increased to 9 mm. These are typical operating conditions at the AWA.

Field maps generated in POISSON ⁴¹ were used to model the solenoid magnets. Two types of rf field maps were used to model the gun and accelerating cavities. 2D maps were generated in SUPERFISH ⁴², and used in the 1 nC case. 3D maps were generated in ACE3P ⁴³, and used

in 40 nC simulations. This is the reason for time-to-solution differences seen in Table 1. While 3D field maps are computationally more expensive to evaluate, they model asymmetries that are present in the AWA rf cavities.

Implementation of Machine Learning Based Surrogate Models The ANNs were implemented in Keras ⁴⁴, with TensorFlow ⁴⁵ as the backend. For general demonstration of the technique, we used a topology and set of hyperparameters that the authors had previously found to work well for similar problems in accelerators ^{28,29,31}. This consisted of a fully-connected, feed-forward ANN with four hidden layers, each with 20 nodes and hyperbolic tangent activation functions. No regularization penalties (e.g. L_1 or L_2 norm) were used on the weights. The ANNs were trained for 10k epochs with a batch size of 500 points. The Adam optimization algorithm ⁴⁶ was used for training, with an initial learning rate of 0.001, $\beta_1 = 0.9$, and $\beta_2 = 0.999$. For training, the random sample data was randomly split into training (60%), validation (20%), and testing (20%) sets. All data sets were scaled to fit within an appropriate range. For example, in the case of an ANN with hyperbolic tangent activation functions, the data was scaled to be within the range of [-1, 1].

For the comparisons shown in Figure 10 and Figure 11, a second fully-connected, feed-forward ANN and set of hyperparameters was selected using a grid search. The grid search consisted of different numbers of layers and nodes, initial learning rates, and regularization parameters. Among all models the one with the smallest validation error based on the test set for 1 nC bunch charge was chosen. While only one weight initialization was used for each network examined (i.e. no random re-starts and subsequent retraining to account for the impact of random weight initial-

izations was used), the resultant prediction error was fairly smooth. The final network consisted of four hidden layers with 12, 24, 48, 96 neurons, hyperbolic tangent activation functions, and no regularization. The model was trained for a total of 30k epochs using Adam ⁴⁶ with an initial learning rate of 0.0001. In addition we increased the batch size after every 6k epochs using the following sizes: 300, 600, 1.2k, 1.8k, 3.6k. The mean squared error was used as the cost function.

The PCE model is built on the Uncertainty Quantification Toolkit (UQtk) ⁴⁷. UQtk is a lightweight C++/Python library that helps perform basic UQ tasks including intrusive and non-intrusive forward propagation. In contrast to the quadrature method of ³⁰, in this work we used the regression method ^{48,49} with Legendre polynomials, and we associate a uniform distribution to all input variables. In this work, we closely follow ³⁰ in regard to the PCE surrogate model. Furthermore, choosing a polynomial order of $p = 4$ and 60% of the random sample for training matches the ANN model most closely.

The GA optimization with the surrogate models is done using the python package DEAP ⁵⁰. The hyperparameters used are the same as the GA optimization directly within OPAL.

ML in the Context of this Work This work is focused on using supervised learning techniques in regression tasks. In a regression problem, a data set consisting of inputs X and outputs Y generated with process f is used to obtain an approximate input-output mapping \tilde{f} . In this work, f is the OPAL based “Physics Model”, such that $Y = f(X)$. Y is also known as the ground truth, or in other words, what we would like our ML model \tilde{f} to be able to predict accurately after training. Training in this case is simply an optimization problem to find parameters θ that minimize the

prediction error (i.e. finding $\operatorname{argmin}_\theta[Y - \tilde{f}(X, \theta)]$). The model should also be able to interpolate, i.e. given $X' \notin X$, find a Y' such that $Y' = f(X')$, thus allowing one to use the model when values not contained in the training set, X , are provided.

Background on Artificial Neural Networks The term ‘‘Artificial Neural Network’’ refers to a broad class of tools within ML that share the common property of consisting of many interconnected processing units that are used to transform data ^{34,35,51,52}. In the simplest case, ANNs are built from a few individual components. The first is an affine linear function $T : \mathbb{R}^n \rightarrow \mathbb{R}^m$, defined as $T(x) := Wx + b$, where $W = (a_{ij}) \in \mathbb{R}^{m \times n}$, $x \in \mathbb{R}^n$, $b \in \mathbb{R}^m$, and $n, m \in \mathbb{N}$. W and b are commonly referred to as the weights and biases of the ANN. The second is an activation function $\sigma : \mathbb{R} \rightarrow \mathbb{R}$, which is typically nonlinear. Many variants of σ exist. Three frequently used activation functions are the rectified linear unit $\sigma(x) = \max(0, x)$, the Sigmoid function $\sigma(x) = (1 + e^{-x})^{-1}$, and the hyperbolic tangent function $\sigma(x) = \frac{2}{1 + \exp[-2x]} - 1$. The activation function is applied in an element-wise manner hence, a vector activation function $\sigma : \mathbb{R}^n \rightarrow \mathbb{R}^n$ can be defined.

Now we are able to define a continuous function $f(x)$ by a composition of linear transforms T^i and activation functions σ , i.e. ,

$$f(x) = T^k \circ \sigma \circ T^{k-1} \circ \sigma \cdots \circ T^1 \circ \sigma \circ T^0(x), \quad (1)$$

with $T^i(x) = W_i x + b_i$. W_i are initially undetermined matrices and b_i initially undetermined vectors and $\sigma(\cdot)$ is the element-wise activation function. The values of W_i and b_i are randomly initialized and adjusted during ‘‘training’’ using an optimization algorithm to maximize some performance

metric. For example, in a regression task on some data set with inputs x and outputs y , this may be the mean squared error between predicted y values from the ANN and the true y values. The dimensions of W_i and b_i are also chosen to optimize the performance of the ANN on a given task.

Such an ANN is called a $(k + 1)$ -layer ANN, which has k hidden layers. Denoting all the undetermined coefficients (e.g., W_i and b_i) in (1) as $\theta \in \Theta$, where θ is a high dimensional vector and Θ is the span of θ , the ANN representation of a continuous function can now be viewed as

$$f = f(x; \theta).$$

Let $\mathbb{F} = \{f(\cdot, \theta) | \theta \in \Theta\}$ denote the set of all expressible functions by the ANN parameterized by $\theta \in \Theta$, then \mathbb{F} provides an efficient way to represent unknown continuous functions.

Approximation properties of neural network can be found in ^{35,53}, where the authors studied approximation properties for the function classes given by a feed-forward neural network with a single hidden layer. In later works, authors studied the error estimates for such neural networks in terms of hyper-parameters such as number of neurons, layers of the network, and activation functions. A good review can be found in ⁵¹ and ³⁴.

Background on Polynomial Chaos Expansion (PCE) We briefly introduce the mathematical basis in the style and the notation of ³⁶. Let $(\Omega, \mathcal{F}, \mathcal{P})$ be a complete probability space, where Ω is the sample set and \mathcal{P} is a probability measure on \mathcal{F} , the σ -field (algebra) or Borel measure. Input uncertainties of the system have been discretised and approximated by the random vector $\boldsymbol{\xi} = (\xi_1, \dots, \xi_d) : \Omega \rightarrow \mathbb{R}^d$, $d \in \mathbb{N}$. The Probability Density Function (PDF) of the random

variable, ξ_k , is denoted by $\rho(\xi_k)$ and, $\rho(\boldsymbol{\xi})$ represents the joint PDF of $\boldsymbol{\xi}$. Let \mathbf{i} be a multi-index $\mathbf{i} = (i_1, \dots, i_d) \in \mathcal{I}_{d,p}$ and the set of multi-indices $\mathcal{I}_{d,p}$ is defined by $\mathcal{I}_{d,p} = \{\mathbf{i} = (i_1, \dots, i_d) \in \mathbb{N}_0^d : \|\mathbf{i}\|_1 \leq p\}$, where $\|\cdot\|_1$ is the l_1 norm i.e., $\|\cdot\|_1 = i_1 + \dots + i_d$, and p is the polynomial order.

All square integrable, second-order random variables with finite variance output, $u(\boldsymbol{\xi}) \in L_2(\Omega, \mathcal{F}, \mathcal{P})$, can be written as

$$u(\boldsymbol{\xi}) = \sum_{|\mathbf{i}|=0}^{\infty} \alpha_{\mathbf{i}} \Psi_{\mathbf{i}}(\boldsymbol{\xi}). \quad (2)$$

Hence $\alpha_{\mathbf{i}}$ denotes the deterministic coefficients and $\Psi_{\mathbf{i}}(\boldsymbol{\xi})$ are the multivariate PC basis functions, ^{36,54}. Note that the uncertain QoI, u , is represented by a vector of deterministic parameters $\alpha_{\mathbf{i}}$. For the truncated PC Expansion (PCE) to order p in d dimensions of (2) we get

$$\hat{u}(\boldsymbol{\xi}) = \sum_{\mathbf{i} \in \mathcal{I}_{d,p}} \alpha_{\mathbf{i}} \Psi_{\mathbf{i}}(\boldsymbol{\xi}). \quad (3)$$

The basis functions $\Psi_{\mathbf{i}}(\boldsymbol{\xi})$ in (3) are generated from

$$\Psi_{\mathbf{i}}(\boldsymbol{\xi}) = \prod_{k=1}^d \Psi_{i_k}(\xi_k), \quad \mathbf{i} \in \mathcal{I}_{d,p}, \quad (4)$$

where $\Psi_{i_k}(\xi_k)$ are univariate polynomials of degree $i_k \in \mathbb{N}_0 := \mathbb{N} \cup \{0\}$, orthogonal with respect to $\rho(\xi_k)$ (see ³⁶, Table 3), i.e., $\mathbb{E}[\Psi_{i_k} \Psi_{j_k}] = \langle \Psi_{i_k} \Psi_{j_k} \rangle = \int \Psi_{i_k}(\xi_k) \Psi_{j_k}(\xi_k) \rho(\xi_k) d\xi_k = \delta_{i_k j_k} \mathbb{E}[\Psi_{i_k}^2]$.

Here $\delta_{i_k j_k}$ denotes the Kronecker delta and $\mathbb{E}[\cdot]$ is the expectation operator.

The number P of PC basis functions of order $P < p$ in dimension d can be calculated by

$$P = |\mathcal{I}_{d,p}| = \frac{(p+d)!}{p!d!}.$$

The PC basis functions $\Psi_i(\boldsymbol{\xi})$ are orthogonal, $\mathbb{E}[\Psi_i\Psi_j] = \delta_{i,j}\mathbb{E}[\Psi_i^2]$, because of the orthogonality of $\Psi_{i_k}(\xi_k)$ and the independence of ξ_k . As $p \rightarrow \infty$, the truncated PC expansion in (3) converges in the mean-square sense, iff the following two conditions are fulfilled: 1) $u(\boldsymbol{\xi})$ has finite variance and 2) the coefficients α_i are computed from the projection equation ⁵⁵

$$\alpha_i = \mathbb{E}[u(\cdot)\Psi_i(\cdot)]/\mathbb{E}[\Psi_i^2]. \quad (5)$$

Non-intrusive methods, as discussed here, use existing deterministic solvers (the physics simulation c.f. Figure 3) as black boxes. First, one needs to generate a set of N deterministic or random samples of $\boldsymbol{\xi}$, denoted by $\{\boldsymbol{\xi}^{(i)}\}_{i=1}^N$. The second step is to generate N realizations of the output QoI, $\{u(\boldsymbol{\xi}^{(i)})\}_{i=1}^N$, with the available deterministic solver. The third and final step is to solve for the PC coefficients using the obtained realizations. As a side product, the mean, $\mathbb{E}[\cdot]$, and variance, $\text{Var}[\cdot]$, of $u(\boldsymbol{\xi})$ can be directly approximated from the PC coefficients because of polynomial basis orthogonality, details can be found in ³⁶. The practical steps for constructing the PCE surrogate model are described in detail in ³⁰.

Another very useful feature is the ability to quantify sensitivities via Sobol' indices, not directly accessible in the case of an ANN model. The first order PC-based Sobol' index, S_k , represents the individual effects of the random input ξ_k on the variability of $u(\boldsymbol{\xi})$, and is given by

$$S_k = \frac{1}{\text{Var}[u(\boldsymbol{\xi})]} \sum_{i \in \mathcal{I}_k} \alpha_i^2 \mathbb{E}[\Psi^2(\xi_i)], \quad \mathcal{I}_k = \{\mathbf{i} \in \mathbb{N}_0^d : i_k > 0, i_{m \neq k} = 0\}.$$

To compute S_k , all random inputs except ξ_k are fixed. As a consequence, S_k does not include effects arising from the interactions between ξ_k and the other random inputs. This also means that \mathcal{I}_k includes only the dimension k .

The fractional contribution to the total variability of $u(\boldsymbol{\xi})$ due to parameter ξ_k , considering all other model parameters, is given by

$$S_k^T = \frac{1}{\text{Var}[u(\boldsymbol{\xi})]} \sum_{i \in \mathcal{I}_k^T} \alpha_i^2 \mathbb{E}[\Psi^2(\xi_i)] \quad \mathcal{I}_k^T = \{\mathbf{i} \in \mathbb{N}_0^d : i_k > 0\}.$$

The set of multi indices \mathcal{I}_k^T includes dimension k among others.

Now we are in a position to rank the importance of the variables. The smaller S_k^T is, the less important the random input, ξ_k , becomes. We note, for the extreme case $S_k^T \ll 1$, the variable ξ_k is considered to be insignificant. In such a case, the variable can be replaced by its mean value without considerable effects on the variability of $u(\boldsymbol{\xi})$.

The sensitivity analysis can not be directly obtained with an ANN and resembles an additional feature of PCE, however in this paper we focus more on the performance of the surrogate models and refer the interested reader to ³⁰.

Code Availability For this research only open source software is used. This includes the accelerator simulation framework OPAL ¹ and Python-based software tools: DEAP ⁵⁰, Keras ⁴⁴, TensorFlow ⁴⁵, UQTK ⁴⁷, and sci-kit learn ⁵⁶. All input files to generate the data of this paper are available upon on request.

1. Adelman, A. *et al.* The OPAL (Object Oriented Parallel Accelerator Library) Framework. Tech. Rep. PSI-PR-08-02, Paul Scherrer Institut (2008-2019).
2. Qiang, J., Lidia, S., Ryne, R. D. & Limborg-Deprey, C. Three-dimensional quasistatic model

- for high brightness beam dynamics simulation. *Phys. Rev. ST Accel. Beams* **9**, 044204 (2006).
3. Qiang, J., Ryne, R. D., Habib, S. & Decyk, V. An object-oriented parallel particle-in-cell code for beam dynamics simulation in linear accelerators. *J. Comput. Phys.* **163**, 434 – 451 (2000).
 4. Floettmann, K. ASTRA: A Space Charge Tracking Algorithm (1997-2017).
 5. Friedman, A. *et al.* Computational methods in the warp code framework for kinetic simulations of particle beams and plasmas. *IEEE Trans. on Plasma Science* **42**, 1321–1334 (2014).
 6. Fonseca, C. M., Paquete, L. & Lopez-Ibanez, M. An improved dimension-sweep algorithm for the hypervolume indicator. In *IEEE Intl. Conf. Evol. Comput.*, 1157–1163 (2006).
 7. Beume, N., Fonseca, C. M., Lopez-Ibanez, M., Paquete, L. & Vahrenhold, J. On the complexity of computing the hypervolume indicator. *IEEE Trans. Evol. Comput.* **13**, 1075–1082 (2009).
 8. Bazarov, I. V. & Sinclair, C. K. Multivariate optimization of a high brightness dc gun photoinjector. *Phys. Rev. ST Accel. Beams* **8**, 034202 (2005).
 9. Hofler, A. *et al.* Innovative applications of genetic algorithms to problems in accelerator physics. *Phys. Rev. ST Accel. Beams* **16**, 010101 (2013).
 10. Neveu, N. *et al.* A parallel general purpose multi-objective optimization framework, with application to beam dynamics. Preprint at <https://arxiv.org/pdf/1302.2889.pdf> (2018).
 11. Chu, C. *et al.* XAL-based applications and online model for LCLS. In *Proc. of PAC*, FR5REP022 (2010).

12. Pelaia, T. Open XAL Status Report 2013. In *Proc. of IPAC*, MOPWO086 (2013).
13. Scheinker, A. & Gessner, S. Adaptive method for electron bunch profile prediction. *Phys. Rev. ST Accel. Beams* **18**, 102801 (2015).
14. Baily, S. A., Pang, X. & Rybarcyk, L. High-performance beam simulator for the lansce linac. In *Proc. of IPAC*, C1205201 (2012).
15. Sun, Y. Multi-Objective Online Optimization of Beam Lifetime at APS. In *Proc. of NAPAC*, WEPOB12 (2017).
16. Bergan, W. F. *et al.* Online storage ring optimization using dimension-reduction and genetic algorithms. Preprint at <https://arxiv.org/abs/1807.10720> (2018).
17. Ryne, R. *et al.* Scidac advances and applications in computational beam dynamics. *J. Phys. Conf. Ser.* **16**, 210 (2005).
18. SciDAC: Scientific Discovery through Advanced Computing.
19. Borland, M. Elegant: A flexible sdds-compliant code for accelerator simulation. Tech. Rep. LS-287, Argonne National Laboratory (2000-2018).
20. Takeda, H. & Stovall, J. E. Modified parmila code for new accelerating structures. In *Proc. of PAC*, vol. 4, 2364–2366 (1995).
21. Adelman, A., Locans, U. & Suter, A. The dynamic kernel scheduler - part 1. *Comput. Phys. Commun.* **207**, 83–90 (2016).

22. Vay, J.-L. Noninvariance of space- and time-scale ranges under a lorentz transformation and the implications for the study of relativistic interactions. *Phys. Rev. Lett.* **98**, 130405 (2007).
23. Vay, J.-L., Haber, I. & Godfrey, B. B. A domain decomposition method for pseudo-spectral electromagnetic simulations of plasmas. *Journal of Computational Physics* **243**, 260 – 268 (2013).
24. Lehe, R., Kirchen, M., Andriyash, I. A., Godfrey, B. B. & Vay, J.-L. A spectral, quasi-cylindrical and dispersion-free particle-in-cell algorithm. *Computer Physics Communications* **203**, 66 – 82 (2016).
25. Conde, M. *et al.* Research program and recent results at the argonne wakefield accelerator facility (AWA). In *Proc. of IPAC, WEPAB132* (2017).
26. Ha, G. *et al.* Perturbation-minimized triangular bunch for high-transformer ratio using a double dogleg emittance exchange beam line. *Phys. Rev. Accel. Beams* **19**, 121301 (2016).
27. Gai, W., Power, J. G. & Jing, C. Short-pulse dielectric two-beam acceleration. *J. Plasma Phys.* **78**, 339345 (2012).
28. Edelen, A., Edelen, J., Biedron, S., Milton, S. & van der Slot, P. Using a neural network control policy for rapid switching between beam parameters in a FEL. In *Proc. of IFEL*, 406–409 (2017).
29. Edelen, A., Edelen, J., Biedron, S., Milton, S. & van der Slot, P. Recent Applications of Neural Networks to Modeling and Control of Particle Accelerators. In *Proc. of IPAC, THYGBE2* (2018).

30. Adelman, A. On uncertainty quantification in particle accelerators modelling. *Accepted for publication in SIAM JUQ*, Preprint at <https://arxiv.org/abs/1509.08130> (2019).
31. Edelen, A., Biedron, S., Edelen, J. & Milton, S. First steps toward incorporating image based diagnostics into particle accelerator control systems using convolutional neural networks. In *Proc. of NAPAC, TUPOA51* (2017).
32. Deb, K., Pratap, A., Agarwal, S. & Meyarivan, T. A fast and elitist multiobjective genetic algorithm: NSGA-II. *IEEE Trans. Evol. Comput.* **6**, 182–197 (2002).
33. Laboratory Computing Resource Center. <https://www.lcrc.anl.gov/>.
34. Pinkus, A. Approximation theory of the mlp model in neural networks. *Acta Numerica* **8**, 143195 (1999).
35. Hornik, K., Stinchcombe, M. & White, H. Multilayer feedforward networks are universal approximators. *Neural Networks* **2**, 359 – 366 (1989).
36. Smith, R. *Uncertainty Quantification: Theory, Implementation, and Applications* (SIAM, 2014).
37. Vapnik, V. *Statistical learning theory*. Adaptive and learning systems for signal processing, communications, and control (Wiley, 1998).
38. Sobol, I. Global sensitivity indices for nonlinear mathematical models and their monte carlo estimates. *Mathematics and Computers in Simulation* **55**, 271 – 280 (2001).

39. Gulliford, C. *et al.* Demonstration of low emittance in the cornell energy recovery linac injector prototype. *Phys. Rev. ST Accel. Beams* **16**, 073401 (2013).
40. Ineichen, Y. *Toward massively parallel multi-objective optimization with application to particle accelerators*. Ph.D. thesis, ETH Diss. 21114 (2013).
41. Warren, J. L., Boicourt, G. P., Menzel, M. T., Rodenz, G. W. & Vasquez, M. C. Revision of and Documentation for the Standard Version of the POISSON Group Codes. *IEEE Trans. Nucl. Sci.* **32**, 2870–2872 (1985).
42. Halbach, K. & Holsinger, R. F. Superfish-a computer program for evaluation of rf cavities with cylindrical symmetry. *Part. Accel.* **7**, 213–222 (1976).
43. Kononenko, O. *et al.* Advances in massively parallel electromagnetic simulation suite ACE3P. In *Proc. of ICAP, FRAJ13* (2016).
44. Chollet, F. *et al.* Keras: The python deep learning library (2015).
45. Abadi, M. *et al.* TensorFlow: Large-scale machine learning on heterogeneous systems (2015).
46. Kingma, D. P. & Ba, J. Adam: A method for stochastic optimization. *CoRR*. Preprint at <https://arxiv.org/abs/1412.6980> (2014).
47. Debusschere, B., Sargsyan, K., Safta, C. & Chowdhary, K. *Uncertainty Quantification Toolkit (UQTK)*, 1–21 (Springer International Publishing, Cham, 2016).
48. Debusschere, B. *et al.* Numerical challenges in the use of polynomial chaos representations for stochastic processes. *SIAM J. Sci. Comput.* **26**, 698–719 (2004).

49. Sudret, B. Global sensitivity analysis using polynomial chaos expansions. *Reliability Engineering & System Safety* **93**, 964 – 979 (2008).
50. Fortin, F.-A., De Rainville, F.-M., Gardner, M.-A., Parizeau, M. & Gagné, C. DEAP: Evolutionary algorithms made easy. *J. Mach. Learn. Res.* **13**, 2171–2175 (2012).
51. Ellacott, S. W. Techniques for the mathematical analysis of neural networks. *J. Comput. Appl. Math.* **50**, 283–297 (1994).
52. Cybenko, G. *Analysis and Design of Neural Networks* (PN, 1992).
53. Cybenko, G. Approximation by superpositions of a sigmoidal function. *Mathematics of Control, Signals and Systems* **2**, 303–314 (1989).
54. Ghanem, R. & Spanos, P. *Stochastic Finite Elements: A Spectral Approach* (Springer-Verlag, 1991, New York).
55. Xiu, D. & Karniadakis, G. The wiener–askey polynomial chaos for stochastic differential equations. *SIAM J. Sci. Comput.* **24**, 619–644 (2002).
56. Pedregosa, F. *et al.* Scikit-learn: Machine learning in Python. *J. Mach. Learn. Res.* **12**, 2825–2830 (2011).

Acknowledgements We gratefully acknowledge the computing resources provided on Bebop, a high-performance computing cluster operated by the Laboratory Computing Resource Center at Argonne National Laboratory. The training of the surrogate models benefited from the ETH Leonard cluster the CSCS Piz-Daint and the SLAC OCIO Jupyter-Hub GPU cluster.

This work was supported by the U.S. Department of Energy, Office of Science, under contract numbers DE-AC02-76SF00515, DE-AC02-06CH11357, and grant number DE-SC0015479.

Competing Interests The authors declare that they have no competing financial interests.

Correspondence Correspondence and requests for materials should be addressed to A.E. (email: eden@slac.stanford.edu) or A.A. (email: andreas.adelmann@psi.ch).

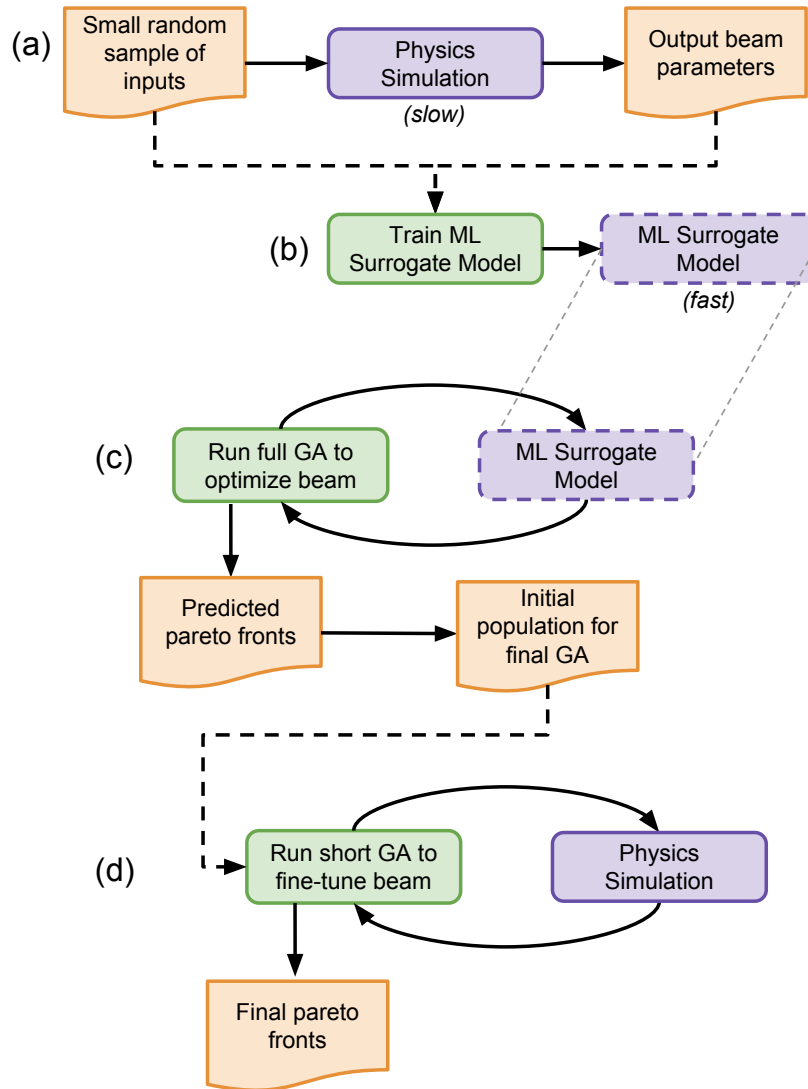


Figure 12: Workflow for method to obtain orders of magnitude faster GA optimization of particle accelerators. First, run a small random sample of inputs through the physics simulation (e.g. a few hundred points in our case) (a). Train an ML surrogate model on the random sample (b). Run the GA with the surrogate model to obtain predictions of the Pareto front and corresponding optimal input settings on the machine (c). Use the predicted optimal input settings as the initial population in a second, shorter GA optimization over the physics simulation to fine-tune and confirm the result (d).